Article

The Origin of Transverse Anisotropy in Axially Symmetric Single Molecule Magnets

Anne-Laure Barra, Andrea Caneschi, Andrea Cornia, Dante Gatteschi, Lapo Gorini, Leo-Philipp Heiniger, Roberta Sessoli, and Lorenzo Sorace

J. Am. Chem. Soc., **2007**, 129 (35), 10754-10762• DOI: 10.1021/ja0717921 • Publication Date (Web): 09 August 2007

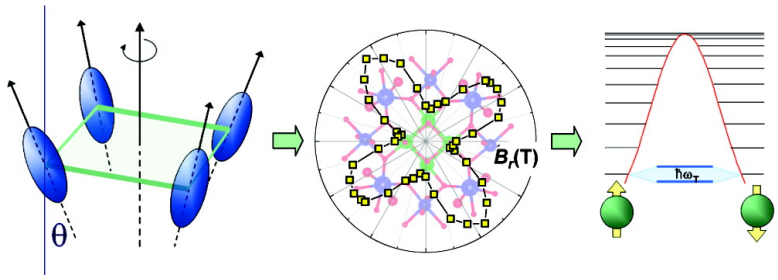

More About This Article

Additional resources and features associated with this article are available within the HTML version:

- Supporting Information
- Links to the 4 articles that cite this article, as of the time of this article download
- Access to high resolution figures
- Links to articles and content related to this article
- Copyright permission to reproduce figures and/or text from this article

View the Full Text HTML

J|A|C|S
ARTICLES
Published on Web 08/09/2007

The Origin of Transverse Anisotropy in Axially Symmetric Single Molecule Magnets

Anne-Laure Barra,[†] Andrea Caneschi,[‡] Andrea Cornia,[§] Dante Gatteschi,*[,‡] Lapo Gorini,[‡] Leo-Philipp Heiniger,[‡] Roberta Sessoli,[‡] and Lorenzo Sorace[‡]

Contribution from the Grenoble High Magnetic Field Laboratory—CNRS, 38042 Grenoble, France, Department of Chemistry & INSTM (UdR Firenze), University of Florence, Sesto Fiorentino, 50019, Italy, and Department of Chemistry & INSTM (UdR Modena), University of Modena and Reggio Emilia, Modena, 41100, Italy

Received March 14, 2007; E-mail: dante.gatteschi@unifi.it

Abstract: Single-crystal high-frequency electron paramagnetic resonance spectroscopy has been employed on a truly axial single molecule magnet of formula $[Mn_{12}O_{12}(^tBu\text{-}CH_2CO_2)_{16}(CH_3OH)_4]\cdot CH_3OH$ to investigate the origin of the transverse magnetic anisotropy, a crucial parameter that rules the quantum tunneling of the magnetization. The crystal structure, including the absolute structure of the crystal used for EPR experiments, has been fully determined and found to belong to $I\bar{4}$ tetragonal space group. The angular dependence of the resonance fields in the crystallographic *ab* plane shows the presence of high-order tetragonal anisotropy and strong dependence on the M_S sublevels with the second-highest-field transition being angular independent. This was rationalized including competing fourth- and sixth-order transverse parameters in a giant spin Hamiltonian which describes the magnetic anisotropy in the ground $S = 10$ spin state of the cluster. To establish the origin of these anisotropy terms, the experimental results have been further analyzed using a simplified multispin Hamiltonian which takes into account the exchange interactions and the single ion magnetic anisotropy of the Mn^{III} centers. It has been possible to establish magneto-structural correlations with spin Hamiltonian parameters up to the sixth order. Transverse anisotropy in axial single molecule magnets was found to originate from the multispin nature of the system and from the breakdown of the strong exchange approximation. The tilting of the single-ion easy axes of magnetization with respect to the 4-fold molecular axis of the cluster plays the major role in determining the transverse anisotropy. Counterintuitively, the projections of the single ion easy axes on the *ab* plane correspond to hard axes of magnetization.

Introduction

Molecules showing slow relaxation of the magnetization at low temperature,[1−3] commonly known as single molecule magnets (SMMs),[4] have represented a major breakthrough in nanomagnetism providing evidence of the coexistence of classical and quantum effects in the dynamics of the magnetization.[5−8] The key parameters characterizing these systems are the large spin values originated by intramolecular exchange interactions between the paramagnetic centers and the easy axis-type magnetic anisotropy, in most cases dominated by the single-ion contributions.[9] Another key feature is the transverse magnetic anisotropy, which influences the quantum tunneling of the magnetization.

In general the low-temperature magnetic properties of SMMs have been interpreted by attributing a well-defined total spin value (S) to the ground state and by using a so-called "giant-spin Hamiltonian" (GSH). Within the GSH formalism the splitting in zero field of the ground state and the related magnetic anisotropy are described using a multipolar series expansion with terms up to $2S$ order in spin operators. In axial symmetry second-order terms do not yield transverse anisotropy which is brought about by fourth- and higher-order terms. Both purely electronic interactions and vibronic coupling can in principle contribute to high-order anisotropy, whose physical origin remains an open question.[10] Higher-order terms up to $2s$ order, where s denotes the value of the individual spins of the cluster,

[†] Grenoble High Magnetic Field Laboratory—CNRS.
[‡] University of Florence.
[§] University of Modena and Reggio Emilia.

(1) Caneschi, A.; Gatteschi, D.; Sessoli, R.; Barra, A.-L.; Brunel, L. C.; Guillot, M. *J. Am. Chem. Soc.* **1991**, *113*, 5873−5874.
(2) Sessoli, R.; Tsai, H. L.; Schake, A. R.; Wang, S.; Vincent, J. B.; Folting, K.; Gatteschi, D.; Christou, G.; Hendrickson, D. N. *J. Am. Chem. Soc.* **1993**, *115*, 1804−1816.
(3) Sessoli, R.; Gatteschi, D.; Caneschi, A.; Novak, M. A. *Nature* **1993**, *365*, 141−143.
(4) Eppley, H. J.; Aubin, S. M. J.; Wemple, M. W.; Adams, D. M.; Tsai, H. L.; Grillo, V. A.; Castro, S. L.; Sun, Z. M.; Folting, K.; Huffman, J. C.; Hendrickson, D. N.; Christou, G. *Mol. Cryst. Liq. Cryst. Sci. Technol., Sect. A* **1997**, *305*, 167−179.
(5) Thomas, L.; Lionti, F.; Ballou, R.; Gatteschi, D.; Sessoli, R.; Barbara, B. *Nature* **1996**, *383*, 145−147.
(6) Friedman, J. R.; Sarachik, M. P.; Tejada, J.; Ziolo, R. *Phys. Rev. Lett.* **1996**, *76*, 3830−3833.
(7) Wernsdorfer, W.; Sessoli, R. *Science* **1999**, *284*, 133−135.
(8) Hill, S.; Edwards, R. S.; Aliaga-Alcalde, N.; Christou, G. *Science* **2003**, *302*, 1015−1018.
(9) Gatteschi, D.; Sessoli, R.; Villain, J. *Molecular Nanomagnets*; Oxford University Press: Oxford, 2006.
(10) Pederson, M. R.; Bernstein, M.; Kortus, J. *Phys. Rev. Lett.* **2002**, *89*, 097202.

10.1021/ja0717921 CCC: $37.00

may result from the projection of the corresponding higher-order single-ion terms on the ground state. However, the latter are often very small,[11,12] and their effect is further reduced by the very small projection coefficients.[13,14] Moreover sizable fourth-order anisotropy terms have been observed in the ground $S = 4$ state of a tetranuclear cluster containing Ni^{II} ions ($s = 1$), for which fourth- and higher-order single-ion contributions are strictly zero.[14] In this case, fourth- and higher-order terms have been shown to directly reflect the multispin nature of the system, depending on the single ion anisotropy. In a perturbative approach, the effect can be described as the admixture of excited spin states into the ground state (the so-called *S*-mixing[15,16]) and implies a departure from the strong-exchange limit.[17]

In this respect, tetranickel(II)[14] and tetrairon(III)[18] clusters have been extensively studied by using high-frequency electron paramagnetic resonance (HF-EPR), which is able to provide a detailed view of the energy splitting of the *S* multiplets.[19−28] However, a direct relation among the transverse anisotropy, the orientation of the hard and intermediate axes, and the geometrical parameters of the molecular structure has not been established up to now. To fill this gap, we have focused on the widely investigated family of Mn12 clusters, which exhibit either rigorous or idealized tetragonal symmetry.

The archetypal Mn12 cluster compound, $[Mn_{12}O_{12}(OAc)_{16}(H_2O)_4]\cdot 4H_2O\cdot 2AcOH$ (Mn12Ac),[1,29] has retained for almost 20 years the record of the highest temperature for the observation of magnetic hysteresis, a record very recently beaten by a Mn6 cluster.[30] Inelastic neutron scattering (INS) experiments on Mn12Ac have shown that the first excited spin state ($S = 9$) is rather close (ca. 43 cm^{-1}) to the ground state ($S = 10$).[31] Since the overall anisotropic splitting of the latter is ca. 45 cm^{-1}, the strong exchange limit is not attained and spin mixing effects could be present. However, Mn12Ac is not the best choice for a detailed single-crystal EPR investigation. In fact in the crystal structure of Mn12Ac disordered acetic acid molecules of crystallization are hydrogen-bonded to coordinated acetate ions, locally inducing a significant distortion from tetragonal symmetry.[32,33] Among the multitude of Mn12 derivatives synthesized and investigated in the past 10 years only a few have shown true axial symmetry.[28,34,35] The derivative obtained by exchanging acetates with the bulkier *t*-butyl-acetates and recrystallizing the product from methanol/diethyl ether, $[Mn_{12}O_{12}(^tBu\text{-}CH_2\text{-}CO_2)_{16}(CH_3OH)_4]\cdot CH_3OH$ (Mn12^{t}BuAc), turned out to have axial symmetry and to be free from fast-relaxing impurities.[28,34,36] For this reason, it is an ideal candidate for accurate investigations using single-crystal HF-EPR spectroscopy aiming to obtain a profound knowledge of higher-order magnetic anisotropy terms.

We have focused our interest on the angular dependence of the EPR resonance field in the hard plane of magnetization of Mn12^{t}BuAc that has been analyzed by using both the GSH and an approximate multispin Hamiltonian (MSH). The results have evidenced the key role played by the noncollinearity of the single-ion easy axes in the determination of high-order terms of the transverse magnetic anisotropy, which are particularly important in the tunneling of the magnetization.

Results and Discussion

Crystal Structure. Preliminary crystallographic data of Mn12^{t}BuAc, including crystal space group and unit cell volume, were communicated by Wernsdorfer et al.,[34] but no complete crystal analysis has been reported. A complete crystal structure determination has then been undertaken to correlate the magnetic anisotropy to the molecular structure (which is reported in Figure 1).

The core of the molecule structurally resembles those of other members of the Mn12 family.[9] It is made up of a central $[Mn^{IV}{}_4O_4]^{8+}$ cubane linked to eight peripheral Mn^{III} ions by eight μ_3-oxo and four carboxylate ligands. Twelve additional carboxylates and four methanol ligands complete the coordination sphere of the Mn^{III} ions which form a $[Mn^{III}{}_8O_8]^{8+}$ twisted ring. Two different Mn^{III} ions are found in the structure, as commonly observed in Mn12 derivatives: Mn(3) is coordinated to two oxo groups which are on their turn connected to the same Mn^{IV} center; on the other hand the two oxo groups coordinated to Mn(2) are bridging toward two different Mn^{IV} centers. The two Mn^{III} centers are Jahn−Teller elongated, the elongated bond

(11) Mossin, S.; Stefan, M.; ter Heerdt, P.; Bouwen, A.; Goovaerts, E.; Weihe, H. *Appl. Magn. Res.* **2001**, *21*, 587−596.
(12) Gatteschi, D.; Sorace, L. *J. Solid State Chem.* **2001**, *159*, 253−261.
(13) Hartmann-Boutron, F.; Politi, P.; Villain, J. *Int. J. Mod. Phys. B* **1996**, *10*, 2577−2637.
(14) Wilson, A.; Lawrence, J.; Yang, E. C.; Nakano, M.; Hendrickson, D. N.; Hill, S. *Phys. Rev. B* **2006**, *74*, No. 140403.
(15) Liviotti, E.; Carretta, S.; Amoretti, G. *J. Chem. Phys.* **2002**, *117*, 3361−3368.
(16) Carretta, S.; Liviotti, E.; Magnani, N.; Santini, P.; Amoretti, G. *Phys. Rev. Lett.* **2004**, *92*, No. 207205.
(17) Bencini, A.; Gatteschi, D. *EPR of Exchange Coupled Systems;* Springer-Verlag: Berlin, 1990.
(18) Accorsi, S.; Barra, A. L.; Caneschi, A.; Chastanet, G.; Cornia, A.; Fabretti, A. C.; Gatteschi, D.; Mortalò, C.; Olivieri, E.; Parenti, F.; Rosa, P.; Sessoli, R.; Sorace, L.; Wernsdorfer, W.; Zobbi, L. *J. Am. Chem. Soc.* **2006**, *128*, 4742−4755.
(19) Barra, A. L.; Caneschi, A.; Gatteschi, D.; Sessoli, R. *J. Am. Chem. Soc.* **1995**, *117*, 8855−8856.
(20) Goldberg, D. P.; Telser, J.; Krzystek, J.; Montalban, A. G.; Brunel, L. C.; Barrett, A. G. M.; Hoffman, B. M. *J. Am. Chem. Soc.* **1997**, *119*, 8722−8723.
(21) Barra, A. L.; Gatteschi, D.; Sessoli, R. *Phys. Rev. B: Condens. Matter Mater. Phys.* **1997**, *56*, 8192−8198.
(22) Hill, S.; Perenboom, J. A. A. J.; Dalal, N. S.; Hathaway, T.; Stalcup, T.; Brooks, J. S. *Phys. Rev. Lett.* **1998**, *80*, 2453−2456.
(23) Barra, A. L.; Gatteschi, D.; Sessoli, R. *Chem.—Eur. J.* **2000**, *6*, 1608−1614.
(24) Collison, D.; Murrie, M.; Oganesyan, V. S.; Piligkos, S.; Poolton, N. R. J.; Rajaraman, G.; Smith, G. M.; Thomson, A. J.; Timko, G. A.; Wernsdorfer, W.; Winpenny, R. E. P.; Mcinnes, E. J. L. *Inorg. Chem.* **2003**, *42*, 5293−5303.
(25) Gatteschi, D.; Barra, A. L.; Caneschi, A.; Cornia, A.; Sessoli, R.; Sorace, L. *Coord. Chem. Rev.* **2006**, *250*, 1514−1529.
(26) Aliaga-Alcalde, N.; Edwards, R. S.; Hill, S. O.; Wernsdorfer, W.; Folting, K.; Christou, G. *J. Am. Chem. Soc.* **2004**, *126*, 12503−12516.
(27) Edwards, R. S.; Hill, S.; Bhaduri, S.; Aliaga-Alcalde, N.; Bolin, E.; Maccagnano, S.; Christou, G.; Hendrickson, D. N. *Polyhedron* **2003**, *22*, 1911−1916.
(28) Chakov, N. E.; Lee, S. C.; Harter, A. G.; Kuhns, P. L.; Reyes, A. P.; Hill, S. O.; Dalal, N. S.; Wernsdorfer, W.; Abboud, K. A.; Christou, G. *J. Am. Chem. Soc.* **2006**, *128*, 6975−6989.
(29) Lis, T. *Acta Crystallogr., Sect. B: Struct. Sci.* **1980**, *36*, 2042−2046.
(30) Milios, C. J; Vinslava, A.; Wernsdorfer, W.; Moggach, S.; Parsons, S.; Perlepes, S. P.; Christou, G.; Brechin E. K. *J. Am. Chem. Soc.* **2007**, *129*, 2754−2755.
(31) Chaboussant, G.; Sieber, A.; Ochsenbein, S.; Gudel, H. U.; Murrie, M.; Honecker, A.; Fukushima, N.; Normand, B. *Phys. Rev. B* **2004**, *70*, No. 104422.
(32) Cornia, A.; Sessoli, R.; Sorace, L.; Gatteschi, D.; Barra, A. L.; Daiguebonne, C. *Phys. Rev. Lett.* **2002**, *89*, No. 257201.
(33) Cornia, A.; Fabretti, A. C.; Sessoli, R.; Sorace, L.; Gatteschi, D.; Barra, A. L.; Daiguebonne, C.; Roisnel, T. *Acta Crystallogr., Sect. C: Cryst. Struct. Commun.* **2002**, *58*, m371−m373.
(34) Wernsdorfer, W.; Murugesu, M.; Christou, G. *Phys. Rev. Lett.* **2006**, *96*, No. 057208.
(35) Zobbi, L.; Mannini, M.; Pacchioni, M.; Chastanet, G.; Bonacchi, D.; Zanardi, C.; Biagi, R.; Del Pennino, U.; Gatteschi, D.; Cornia, A.; Sessoli, R. *Chem. Commun.* **2005**, 1640−1642.
(36) (a) Hill, S.; Anderson, N.; Wilson, A.; Takahashi, S.; Petukhov, K.; Chakov, N. E.; Murugesu, M.; North, J. M.; Del, Barco, E.; Kent, A. D.; Dalal, N. S.; Christou, G. *Polyhedron* **2005**, *24*, 2284−2292. (b) Hill, S.; Anderson, N.; Wilson, A.; Takahashi, S.; Chakov, N. E.; Murugesu, M.; North, J. M.; Dalal, N. S.; Christou, G. *J. Appl. Phys.* **2005**, *97*, No. 10M510.

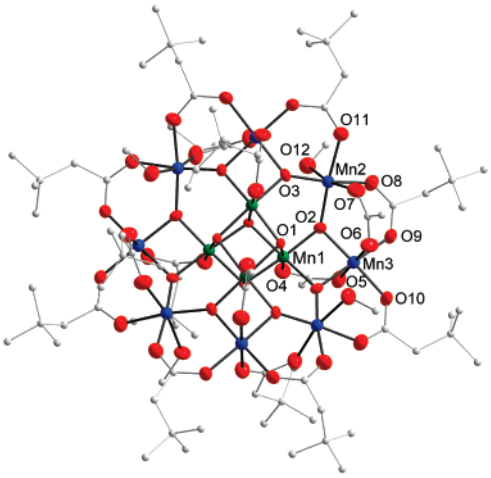

Figure 1. ORTEP view of the molecular structure of $[Mn_{12}O_{12}(^tBu-CH_2-CO_2)_{16}(CH_3OH)_4]\cdot 2CH_3OH$. Mn^{III} sites are reported in blue, Mn^{IV} in green, oxygen in red, and carbon atoms in pale gray. Three *tert*-butyl groups in the labeled region have been omitted for clarity sake.

directions being O(7)−Mn(2)−O(12) and O(5)−Mn(3)−O(6). As observed in other Mn12 derivatives, the two elongation directions form largely different angles with respect to the tetragonal axis, namely ca. 35° for Mn(2) and ca. 11° for Mn(3). Selected structural parameters of Mn12^{t}BuAc and a view of the crystal packing are reported as Supporting Information, SI (Table S1 and Figure S1).

An important feature of Mn12^{t}BuAc is that disorder effects in the crystal lattice are greatly reduced compared to Mn12Ac. In the former, the methanol solvate molecule is found disordered around a 4-fold axis, but it is not hydrogen-bound to the Mn12 moiety. In fact, the closest intermolecular contact of 2.91 Å is observed between a methyl hydrogen atom of the solvent molecule and a hydrogen atom of *tert*-butyl groups. In freshly crystallized samples stored at low-temperature virtually no disorder is observed in the cluster moiety, whose crystallographic symmetry is thus really S_4. On the other hand, in aged samples the occupancy factor of the methanol carbon atom refines to a value much smaller than unity, thus suggesting a partial substitution of methanol with water molecules.

Particular attention has been devoted to resolve a poorly addressed issue in all previous investigations on high-symmetry Mn12 clusters. Although the Mn12 molecule is not chiral (because of its S_4 symmetry), the $I\bar{4}$ space group is acentric and the orientation of the molecules inside the crystal can be determined unambiguously only if the absolute structure is known. The crystal used for X-ray crystal structure gave a final Flack parameter[37] of 0.04(3) but was far too small for HF-EPR investigations. To perform the HF-EPR study, we have then used a larger crystal, which was subsequently analyzed by X-ray diffraction. Its structure has been refined to $R1 = 11.32\%$ for 3280 reflections with $F_o > 4\sigma(F_o)$, which allowed us to unambiguously establish the absolute structure (Flack parameter $= -0.11(5)$ as compared with 1.02(6) for the inverted model). Noticeably, racemic twinning of large crystals, which often occurs in Mn12Ac, was never observed in Mn12^{t}BuAc.

(37) Flack, H. D. *Acta Crystallogr., Sect. A: Found. Crystallogr.* **1983**, *39*, 876−881.

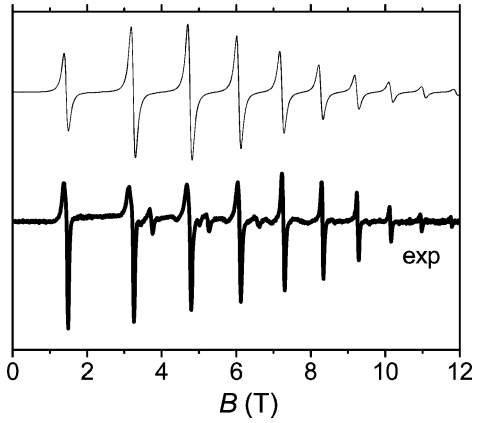

Figure 2. First derivative HF-EPR spectrum recorded at 30 K and 345 GHz on a single crystal of Mn12^{t}BuAc with the field along the *c* crystallographic axis. The thinner line represents the simulated spectrum using GSH (1).

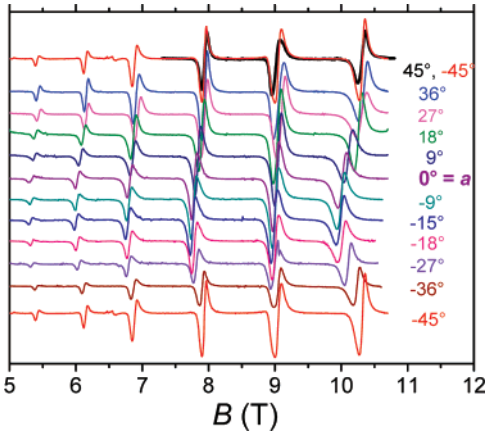

Figure 3. First derivative HF-EPR spectra recorded at 5 K and 115 GHz when the field is applied in the *ab* crystallographic plane at a variable angle Φ from the *a* crystallographic axis.

HF-EPR Spectra. The EPR spectrum obtained with the static magnetic field along the *c* crystallographic axis at 30 K and 345 GHz is reported in Figure 2.

In the investigated field range 10 main lines are observed that can be attributed to transitions between M_S levels of the $S = 10$ ground manifold. Weaker signals are also observed in between the main lines. The temperature dependence of their intensities (see Figure S2 in SI) suggests that they originate from transitions within the first excited-spin multiplet ($S = 9$). With respect to the spacing between the lines and the line width, the obtained spectra are qualitatively fully compatible with those previously reported by Hill et al.[36] In Figure 3 we report the angular dependence of the spectra recorded at 5 K and 115 GHz by placing the crystal on a horizontal rotator in a vertical solenoid (Faraday configuration) and by rotating it around the *c* crystallographic axis. The static magnetic field is applied at an angle Φ from the *a* crystallographic axis. The reported spectra show six well resolved lines, whose intensity decreases going from high to low field as expected for perpendicular transitions when the zero field splitting (zfs) *D* parameter is negative. The angular dependence shows that the spectra at −45° and +45° are superimposable, confirming the expected fourfold symmetry and indicating that the rotation is indeed occurring around the *c*-axis with a negligible misalignment (≤1°).

The highest field signal, that is associated to the $M_S = -10 \rightarrow M_S = -9$ transition, shows the largest angular variation going from $B_r = 10.3$ T at 39° to 9.95 T at −6°. On the contrary the second highest field resonance shows almost no angular dependence, as clearly evidenced in Figure 4a, where we report the resonance fields as a function of the angle for the first five lines.

This anomalous behavior is not related to the parity of the transition because the angular dependence is re-established for resonances at lower field even if the amplitude of the oscillation decreases on going toward the center of the spectrum.

A control experiment performed at 142 GHz, the highest available frequency compatible with the maximum field of the superconducting magnet (12 T), showed that a similar behavior is observed at this frequency. No direct comparison with literature is possible as the angular dependence in the hard plane has been reported only for lines very close to the center of the spectrum.[36]

Simulations of the HF-EPR Spectra with Giant-Spin Hamiltonian. The giant-spin Hamiltonian (GSH) compatible with the tetragonal symmetry of the crystal and including up to the sixth-order terms is given by[38]

$$\mathscr{H} = \mu_B \mathbf{B}\cdot\mathbf{g}\cdot\hat{S} + D\hat{S}_z^{\,2} + B_4^0\hat{\mathbf{O}}_4^0 + B_6^0\hat{\mathbf{O}}_6^0 + B_4^4\hat{\mathbf{O}}_4^4 + B_6^4\hat{\mathbf{O}}_6^4 \quad (1)$$

where the $\hat{\mathbf{O}}_n^m$ operators are defined as

$$\hat{\mathbf{O}}_4^0 = 35\hat{S}_z^{\,4} - 30S(S+1)\hat{S}_z^{\,2} + 25\hat{S}_z^{\,2} + 3S^2(S+1)^2 - 6S(S+1) \quad (2)$$

$$\hat{\mathbf{O}}_4^4 = \{\hat{S}_+^{\,4} + \hat{S}_-^{\,4}\}/2 \quad (3)$$

$$\hat{\mathbf{O}}_6^0 = 231\hat{S}_z^{\,6} - 315S(S+1)\hat{S}_z^{\,4} + 735\hat{S}_z^{\,4} + 105S^2(S+1)^2\hat{S}_z^{\,2} - 525S(S+1)\hat{S}_z^{\,2} + 294\hat{S}_z^{\,2} - 5S^3(S+1)^3 + 40S^2(S+1)^2 - 60S(S+1) \quad (4)$$

$$\hat{\mathbf{O}}_6^4 = {}^1/_4\{(11\hat{S}_z^{\,2} - S(S+1) - 38)(\hat{S}_+^{\,4} + \hat{S}_-^{\,4}) + (\hat{S}_+^{\,4} + \hat{S}_-^{\,4})(11\hat{S}_z^{\,2} - S(S+1) - 38)\} \quad (5)$$

To understand the unusual angular dependence of the HF-EPR lines in the hard plane, a first necessary step is to obtain spin-Hamiltonian parameters as accurate as possible. We started from the spin-Hamiltonian parameters available in the literature for Mn12^{t}BuAc,[36] $g_{\|} = 2.0$, $g_{\perp} = 1.94$, $D = -0.462$ cm^{-1}, $B_4^0 = -2.5 \times 10^{-5}$ cm^{-1}, $B_4^4 = \pm 4.3 \times 10^{-5}$ cm^{-1}. These values nicely fit the low-field lines when the magnetic field is applied parallel to the tetragonal axis. However, starting from the $M_S = -7 \rightarrow M_S = -6$ transition a significant deviation between experiment and simulation is observed. We have then included a nonzero axial sixth-order term, which led to a significant improvement of the fit. These new parameters are then used as input values for a simultaneous fitting procedure[39] of the whole set of measurements (obtained for the magnetic field along the tetragonal axis and for the magnetic field applied at different Φ angles in the hard plane). This procedure resulted in the determination of the transverse parameters up to the sixth order (B_4^4 and B_6^4). The best set of parameters, with $g_{\|} = 2.00$ and $g_{\perp} = 1.93$, determined from the fit is: $D = -0.459(1)$ cm^{-1}, $B_4^0 = -2.34(4) \times 10^{-5}$ cm^{-1}, $B_6^0 = -1.0(2) \times 10^{-8}$ cm^{-1}, $B_4^4 = +2.0(2) \times 10^{-5}$ cm^{-1}, $B_6^4 = -1.0(1) \times 10^{-7}$ cm^{-1}, where the ESD values on the last significant digit are given in parentheses. The axial terms are equivalent to $\alpha = -0.394$ cm^{-1}, $\beta = -4.8 \times 10^{-4}$ cm^{-1}, $\gamma = -2.3 \times 10^{-6}$ cm^{-1} when using for the axial part the Hamiltonian in the form

$$\mathscr{H}_{ax} = \alpha\hat{S}_z^{\,2} + \beta\hat{S}_z^{\,4} + \gamma\hat{S}_z^{\,6} \quad (6)$$

The relations between these parameters and those of the spin Hamiltonian (1) are

$$\alpha = D - 3275B_4^0 + 1213044B_6^0 \quad (7a)$$

$$\beta = 35B_4^0 - 33915B_6^0 \quad (7b)$$

$$\gamma = 231B_6^0 \quad (7c)$$

Notably, the inclusion of the sixth order transverse term $\hat{\mathbf{O}}_6^4$ is necessary to reproduce the angular dependence of the resonance fields in the hard plane. The isotropic nature of the $M_S = -9 \rightarrow M_S = -8$ line requires B_4^4 and B_6^4 to have different signs, with $B_6^4/B_4^4 \approx -0.5 \times 10^{-2}$. The simulation of all the resonance positions is plotted in Figure 4a, showing an acceptable agreement for this type of simulation, while the calculated spectra are given in Supporting Information (Figure S3). The intensity pattern of the spectra is also well accounted for by our simulation.

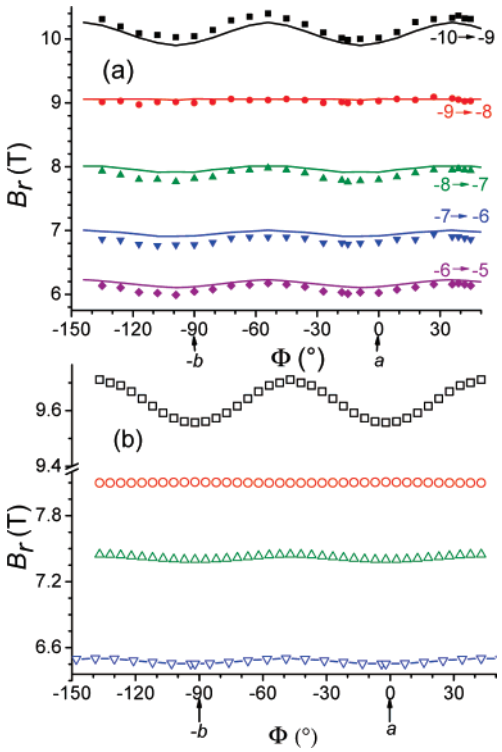

Figure 4. (a) Angular dependence of the resonance field in the HF-EPR spectra recorded at 5 K and 115 GHz when the field is applied in the *ab* crystallographic plane (data of Figure 3). The solid lines represent the calculated resonance fields using the GSH (1). (b) Resonance fields calculated with the MSH (8) on the basis of the five-spin model described in the text (same color code as Figure 4a).

(38) Abragam, A.; Bleaney, B. *Electron paramagnetic resonance of transition ions;* Dover: New York, 1986.
(39) Tregenna-Piggott, P. L. W.; Weihe, H.; Bendix, J.; Barra, A. L.; Güdel, H. U. *Inorg. Chem.* **1999**, *38*, 5928−5929.

A modulation of the EPR lines as a function of Φ, arising from the B_4^4 and B_6^4 parameters, is expected up to the highest frequencies, as shown by perturbation theory (see SI). However, the amplitude and phase of the modulation are strongly frequency dependent. When the strong-field limit is not reached, as in the present case, numerical diagonalization of the GSH matrix is mandatory for an accurate reproduction of the observed angular dependencies.

Multispin Hamiltonian Calculations. The origin of the fourth- and sixth-order parameters evidenced in the previous section is an open question. To gain insight in the role of the local anisotropy on the anisotropy of the cluster we used a multispin Hamiltonian (MSH), a more fundamental Hamiltonian which takes into account the single-ion anisotropy, the magnetic exchange, and the Zeeman interaction at the level of the individual spins. Although eight of the local spins have $s = 2$, and therefore they allow for local fourth-order terms,[11,40] their effect is expected to be negligible because of the combined effect of their small magnitude and the very small projection coefficient on the total spin.[13] We therefore retained only second-order single ion terms, D and E, to investigate the role of S-mixing.[15,16,18]

Unfortunately full diagonalization of the MSH is beyond any computer capability given the $10^8 \times 10^8$ dimensions of the Hilbert space associated to 8 spins $s = 2$ of Mn^{III} and 4 spins $s = {}^3/_2$ of Mn^{IV}. A more sophisticated approach based on sparse matrices diagonalization methods has been recently employed to evaluate axial spin Hamiltonian parameters in Mn12 clusters, but it has not been applied to the analysis of transverse terms.[41] Furthermore, the exchange coupling pattern in Mn12 clusters remains to be fully clarified.[42−44] We thus decided to develop a simplified model, as the essential relationship between local anisotropies and transverse terms should not depend on the details of the exchange coupling situation. Our model was inspired by the observation that a tilting of the local easy axes is required for the occurrence of magnetic anisotropy in the *ab* plane, as also recognized by Hill et al.[14] Hence, the dominant contribution must be provided by Mn(2) ions, whose Jahn−Teller axes form the largest angle with *c*. The Mn(1) and Mn(3) ions are then considered to be fully coupled to give an intermediate spin $s_5 = 2$ with axial anisotropy, which is assumed to interact ferromagnetically with the remaining four Mn(2) spins ($s_1 = s_2 = s_3 = s_4 = 2$). This model is schematized in Figure 5.

In this case the ground state is $S = 10$ with two excited $S = 9$ spin states whose energy separation from the ground state depends on J_p and J_d, the exchange-coupling constants that describe peripheral and diagonal interactions, as shown in Figure 5. Given that these coupling constants have no direct relation with the real exchange interactions active in the cluster, we have assumed for the sake of simplicity $J_p = J_d = J$. The J value has been adjusted to have a $|10,\pm10\rangle \rightarrow |9,\pm9\rangle$ separation that corresponds to the value experimentally observed in INS experiments on Mn12Ac,[31] as data on Mn12^{t}BuAc are not available. No major differences are however expected between exchange interactions in the two compounds. We want to stress that this adjustment could over-estimate the spin-mixing effects as, in the real system, the $S = 9$ spin state with the correct symmetry to promote spin-mixing is not necessarily the closest one to the ground state.[41] However this does not invalidate our qualitative interpretation.

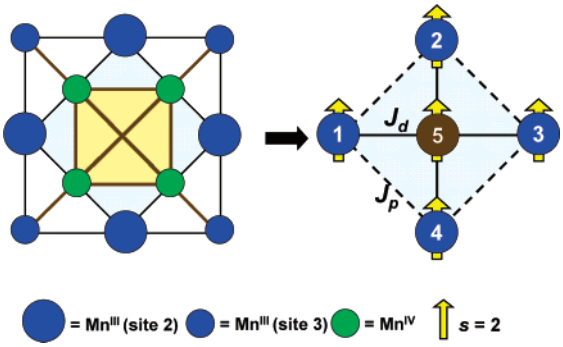

Figure 5. Scheme of the simplified five-spin model for Mn12^{t}BuAc. The eight paramagnetic centers, corresponding to doubly oxo-bridged Mn^{III}−Mn^{IV} pairs, connected by red lines on the left scheme have been approximated with an effective $s = 2$ center with axial symmetry, the brown sphere on the right.

The magnetic anisotropy of the remaining Mn^{III} spins (i.e., Mn(2) atoms in Figure 1) has been evaluated through an angular overlap model (AOM) calculation of the ligand field.[45] We used the same electronic parameters employed for the rationalization of magnetic anisotropy in Mn12Ac,[12,31] whereas the relative positions of the ligating atoms were obtained from the X-ray molecular structure of Mn12^{t}BuAc. The calculations suggest an easy axis anisotropy with a small rhombicity ($D_{Mn^{III}} = -3.17$ cm^{-1} $E_{Mn^{III}} = 0.025$ cm^{-1}). The easy axis direction makes an angle $\theta = 36.4°$ with the tetragonal axis, and deviates by 1.6° from the best-fit line passing through the O(7)−Mn(2)−O(12) direction. These results, substantially similar to those obtained for Mn12Ac,[28] allowed us to build up the complete zfs tensor in the crystallographic reference frame which was used in the analysis reported below. The AOM calculations give for fourth-order terms an upper limit estimate of $B_4^0 = 1.2 \times 10^{-4}$ cm^{-1} and $B_4^4 = -5 \times 10^{-3}$ cm^{-1}, which give a negligible contribution to the cluster fourth-order terms.[13]

It is important to stress here that not only the $D_{Mn^{III}}$ and $E_{Mn^{III}}$ values but also the orientation of the zfs tensor with respect to the crystal reference frame has been taken into account. From the calculated zfs tensor of spin 1 (Figure 5, right) the tensors of the other three symmetry-related Mn^{III} sites have been obtained by applying the symmetry operations of S_4 point group. Thus the full Hamiltonian of the simplified five-spin model is written as

$$H = J[(\sum_{i=1,4} \hat{s}_i \cdot \hat{s}_5) + \hat{s}_1 \cdot \hat{s}_4 + \hat{s}_1 \cdot \hat{s}_2 + \hat{s}_2 \cdot \hat{s}_3 + \hat{s}_3 \cdot \hat{s}_4] + \sum_{i=1,4} \hat{s}_i \cdot \mathbf{R}_i \cdot \mathbf{D}_{Mn^{III}} \cdot \mathbf{R}_i^{-1} \cdot \hat{s}_i + \hat{s}_5 \cdot \mathbf{D}' \cdot \hat{s}_5 + \mu_B \sum_{i=1,5} \mathbf{B} \cdot \mathbf{g}_i \cdot \hat{s}_i \quad (8)$$

where $\mathbf{R}_i$ are the matrices representing the symmetry operations of S_4 point group, and $\mathbf{D}_{Mn^{III}}$ the zfs tensor of the individual $s = 2$ sites. The numbering scheme is the same as in Figure 5.

(40) Gerritsen, H. J. C.; Sabisky, E. S. *Phys. Rev.* **1963**, *132*, 1507.
(41) Waldmann, O.; Gudel, H. U. *Phys. Rev. B* **2005**, *72*, No. 094422.
(42) Raghu, C.; Rudra, I.; Sen, D.; Ramasesha, S. *Phys. Rev. B* **2001**, *64*, 4419.
(43) Regnault, N.; Jolicoeur, T.; Sessoli, R.; Gatteschi, D.; Verdaguer, M. *Phys. Rev. B* **2002**, *66*, No. 054409.
(44) Tupitsyn, I.; Barbara, B. *Magnetism: Molecules to Materials III: Nanosized Magnetic Materials*; Miller, J. S., Drillon, M., Eds.; Wiley-VCH: Weinheim, Germany, 2002, pp 109−168.
(45) Bencini, A.; Ciofini, I.; Uytterhoeven, M. G. *Inorg. Chim. Acta* **1998**, *274*, 90.

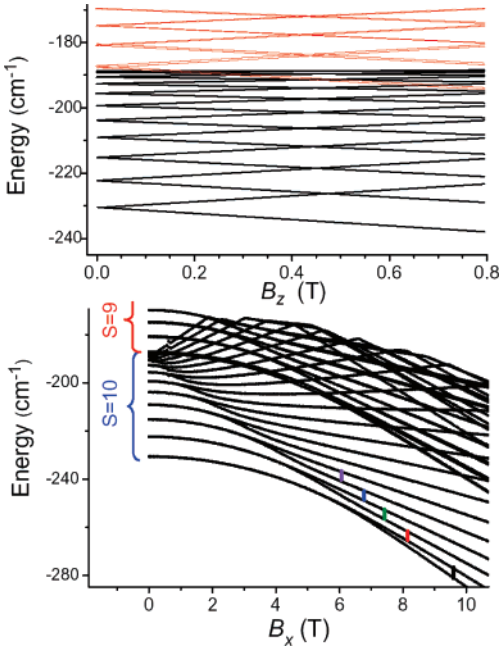

Figure 6. Field dependence of the lowest 35 states calculated for five interacting $s = 2$ spins with the parameters indicated in the text. In the upper part the field is applied along the tetragonal axis, and the 21 states that can be associated with the ground $S = 10$ state of the GSH are reported in black. In the lower part the transverse field dependence is reported, and the EPR transitions investigated in detail are shown with the same color code of Figure 4.

The zfs tensor of the central spin on site 5 (**D**′) is obviously assumed to be axial and its D' parameter has been adjusted so that the ground $S = 10$ is characterized by an overall anisotropy comparable to that experimentally observed.

In Figure 6 we report the energies of the lowest lying states as a function of the magnetic field applied along the *c* and the *a* crystallographic axes, calculated assuming $J = -6.3$ cm^{-1}, $D' = -7.5$ cm^{-1}, and the $\mathbf{D}_{\mathrm{Mn^{III}}}$ tensor obtained by AOM calculations. Even if the energy levels obtained through the full diagonalization of the (3125 × 3125) matrix cannot be rigorously labeled with total spin quantum numbers, the lowest-lying levels strongly resemble the $S = 10$ multiplet with negative zfs typical of Mn12 clusters. Two almost degenerate $S = 9$ states are found close in energy in zero field, and the $|10,\pm10\rangle \rightarrow |9,\pm9\rangle$ separation corresponds to 42.5 cm^{-1} as experimentally observed in INS experiments on Mn12Ac. The total splitting of the levels formally belonging to the ground $S = 10$ multiplet is ca. 41 cm^{-1}.

The presence of high-order transverse anisotropy is evident upon inspection of the calculated energy values in zero field. Even if we take into account the limited precision of the diagonalization of a (3125 × 3125) matrix it is apparent that the states $\pm M_S$ remain degenerate for odd M_S, but are nondegenerate for even M_S. This is fully consistent with the fourfold symmetry of our model. In fact fourth- and higher-order transverse anisotropy terms of the type $\hat{\mathbf{O}}_n^4$ couple states differing by multiples of 4, which is possible for even-M_S but not for odd-M_S states. The amplitude of the splitting in even-M_S pairs is directly related to the higher-order transverse anisotropy.

We have therefore decided to investigate the dependence of this energy splitting on several parameters, like the exchange interaction, the transverse anisotropy of the Mn(2) sites, and the tilting angle θ of the local easy axis with respect to the fourfold molecular axis. The larger is the exchange interaction, and thus the energy separation of the excited-spin states, the smaller is the energy splitting of the $\pm M_S$ pairs, as reported in Figure 7a for the nominally $M_S = \pm4$ pair. It has been previously shown that the *S*-mixing effects responsible for the fourth-order terms vary as D/J.[15] Since the energy splitting between the $M_S = \pm4$ pair involves a $\Delta M_S = 8$, the perturbation acts at the second order and thus a linear dependence of ΔE on $1/J^2$ is expected, as indeed observed in our calculation. As for the rhombic anisotropy of the isolated spins, a variation of E/D from 0 to 0.15 just affects the splitting $\Delta E(M_S = \pm4)$ for a factor of 2 (see Figure S4). In this respect, the key parameter appears to be the misalignment of the local easy direction with respect to the cluster symmetry axis, as shown in Figure 7b, where the splitting of the $M_S = \pm4$ pair is reported as a function of θ. It is apparent that when the local easy axes lie close to the tetragonal axis the splitting, and thus the transverse anisotropy, vanishes.

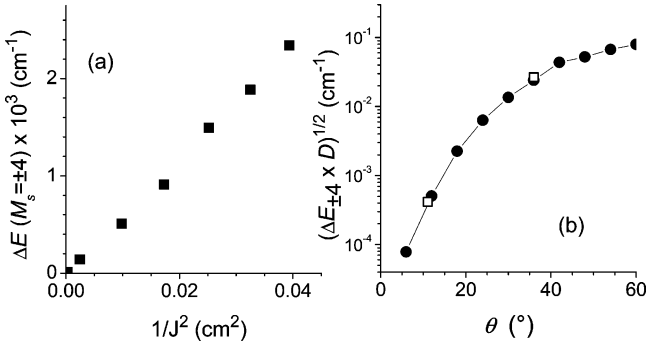

Figure 7. (a) Dependence of the calculated energy splitting between the nominal $M_S = \pm4$ states on the square of the exchange parameter *J* in MSH (8) of the five spins model. (b) The same splitting is evaluated as a function of the tilting angle of the Mn^{III} easy axis. The values for the angles observed for Mn(2) and Mn(3) sites in the crystal structure are reported as open squares.

Here again a perturbative treatment suggests that the fourth-order transverse anisotropy splits the $\pm M_S$ pair of a quantity that is proportional to $D(B_4^4/D)^{M_S/2}$.[13] Therefore by plotting $(\Delta E_{\pm4}D)^{1/2}$ we can have a first insight on the effect of the tilting angle on the transverse anisotropy term, which appears to increase rapidly with the θ angle, as expected.

The splitting in zero field of the $M_S = \pm4$ states demonstrates the occurrence of transverse anisotropy terms, but does not provide any information about the orientation of the hard and intermediate axes in the *ab* plane. Hard and intermediate axes are expected to be found at 45° from each other with 90° periodicity given the tetragonal symmetry of the molecule and to be related to the projection of the single ion easy axes on the *ab* crystallographic plane. However, it is interesting to check whether the projections of the local anisotropy of Mn(2) do indeed correspond to the intermediate or to the hard principal directions. To accomplish this task, and also to compare the results of our calculation with the experimental EPR data, we included the diagonalization procedure in an iterative routine to find the EPR resonance fields at 115 GHz. The results, reported in Figure 4b, show that the largest resonance field is calculated at $\Phi = 43° + n90°$. This angle corresponds to the projection on the *ab* plane of the principal anisotropy axis of Mn(2) as estimated from the AOM calculation.

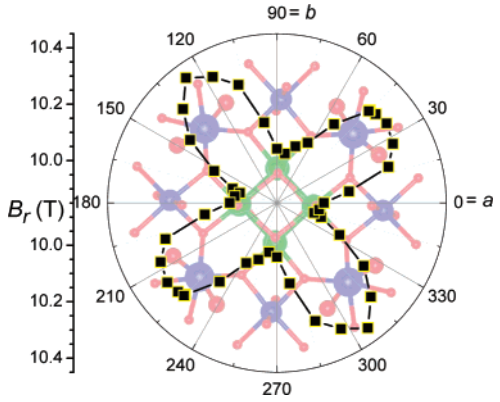

Figure 8. Experimental angular dependence of the $M_S = -10 \rightarrow M_S = -9$ transition in a polar plot superimposed to the absolute structure of Mn12^{t}BuAc obtained for the same crystal used in the HF-EPR experiments. Mn^{IV} is reported in green while large blue spheres evidence the Mn^{III} sites that have been considered in the five spins model calculation. The oxygen atoms highlighted by larger red spheres are those determining the Jahn−Teller elongation axis of the Mn^{III} site included in the calculation.

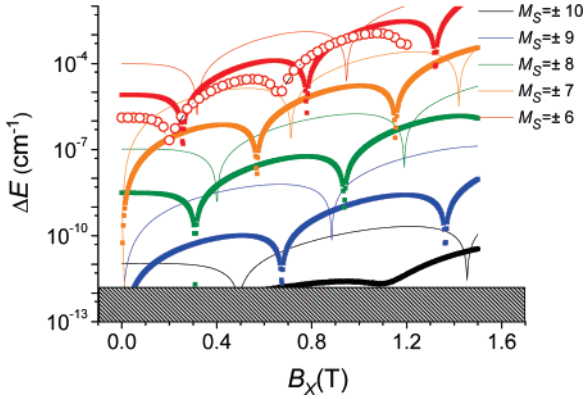

Figure 9. Calculated splitting in zero longitudinal field of the nominal $\pm M_S$ pairs with the GSH up to the sixth order (solid circles) and with the GSH up to the fourth order according to ref 36 (thin lines). The color code for the resonances is given in the legend. The open symbols represent the calculated $M_S = \pm 6$ splitting using the MSH. The shaded area represents the resolution limit imposed by our double precision 64-bit diagonalization procedure.

The Φ angles leading to the largest resonance fields involve a minimal Zeeman splitting of the levels and thus correspond to the hard magnetic directions. That the projections of easy axes correspond to hard magnetic directions may appear counterintuitive but is indeed well evidenced experimentally by superimposing the crystal structure on the polar plot of the experimentally observed $M_S = -10 \rightarrow M_S = -9$ transition, as shown in Figure 8.

A striking feature is evidenced in Figure 4b: the anomalous behavior of the second highest field resonance, the one nominally corresponding to the $M_S = -9 \rightarrow M_S = -8$ transition in the GSH is well accounted for by our model. In fact no angular dependence is calculated for this resonance.

The qualitative agreement of our approximate calculation with the observed behavior is very good, as it reproduces the angular position of the extremes as well as the angular independence of the second transition. We remind that no adjustable parameters have been introduced as far as the contribution to the transverse anisotropy is concerned. Also, neglecting the contribution of the less tilted Mn^{III} sites seems a reasonable approximation.

The simulation of the HF-EPR spectra within the GSH has shown that the isotropic nature of the $M_S = -9 \rightarrow M_S = -8$ transition in the hard plane comes from an accidental balancing of the effects of the $\hat{\mathbf{O}}_4^4$ and $\hat{\mathbf{O}}_6^4$ terms of the spin Hamiltonian. It is interesting to investigate if this accidental condition is correlated with the molecular structure. We have therefore allowed the tilting angle θ to deviate by $\pm$ 5° from the value observed in the crystal structure of Mn12^{t}BuAc. The results, reported in Figure S5 of SI show that such a change in the θ angle is enough to suppress this effect. The calculated resonance fields for different θ values have been simulated with the GSH and the complete set of parameters is given in SI, Table S2. On increasing the θ angle the absolute values of B_4^4 and of B_6^4 increase but the latter less rapidly, thus $|B_6^4|/|B_4^4|$ ratio decreases from 8.5×10^{-3} for $\theta = 31.5°$ to 4.2×10^{-3} for $\theta = 41.5°$.

Tunnel Splitting Evaluation. The transverse high order GSH terms have paramount relevance in the low-temperature dynamics of SMMs. In the low-temperature regime the mechanism of relaxation of the magnetization is mainly determined by an under-barrier process, whose efficiency is directly related to the extent of admixing between states on opposite sides of the barrier. This admixing reflects in level repulsion, whose amplitude is directly related to the tunneling rate, which is minimum for the levels deepest in the well. Moreover this tunnel splitting is strongly sensitive to the application of a transverse field, which, if applied along the hard direction, produces oscillations in the tunnel splitting as a consequence of topological interferences in the tunneling pathways.[7,46,47] These oscillations reflect a fundamental theorem of quantum mechanics[9,48] and have been employed to investigate parity effects in the tunneling of the magnetization of integer and half-integer spin systems.[49]

To evaluate the effects on the tunnel splitting of the sixth-order transverse terms, here for the first time experimentally determined and rationalized, we have plotted in Figure 9 the tunnel splitting for M_S pairs in zero longitudinal field as a function of the transverse field applied along the hard axis. The results obtained using the GSH parameters up to the sixth-order determined here are compared to those computed with the values up to the fourth order previously suggested.[36]

Given the form of $\hat{\mathbf{O}}_6^4$ its inclusion does not alter the overall symmetry provided by $\hat{\mathbf{O}}_4^4$, and thus $\pm M_S$ pairs are degenerate in zero field for odd values of M_S. However, $\hat{\mathbf{O}}_6^4$ significantly affects the tunnel splitting. In particular, the opposite signs of B_4^4 and B_6^4 and the amplified effect of $\hat{\mathbf{O}}_6^4$ on the energies of the levels with large $|M_S|$ lead to a significant reduction of the tunnel splitting for the lowest doublet with a flattening of the oscillations induced by the transverse field. Unfortunately no data are available for the pure tunneling regime of high-symmetry Mn12 clusters because of their very slow tunneling in zero longitudinal field.

It is interesting to compare the tunnel splittings calculated on the basis of the GSH with those evaluated on the basis of MSH. The simplified five spins model has in fact been able to reproduce quite well the transverse anisotropy that is at the origin

(46) Garg, A. *Europhys. Lett.* **1993**, *22*, 205.
(47) Villain, J.; Fort, A. *Eur. Phys. J.* **2000**, *17*, 69−83.
(48) von Neumann, J.; Wigner, E. P. *Phys. Z* **1929**, *30*, 467.
(49) Wernsdorfer, W.; Chakov, N. E.; Christou, G. *Phys. Rev. Lett.* **2005**, *95*, No. 037203

of the quantum tunneling of the magnetization. The large dimension of the spin Hamiltonian matrix does not allow the necessary precision in the eigenvalues to evaluate the tunnel splitting of the lower doublets. We have therefore reported in Figure 9 the transverse field dependence of the tunnel splitting of the nominally $M_S = \pm 6$ pair. At variance with previous findings for other systems[16] the tunnel splitting thus evaluated is smaller than that obtained with the GSH.

Conclusions

In this paper, we have presented a detailed EPR single-crystal study of Mn12^{t}BuAc, a Mn12 derivative with exact S_4 molecular symmetry. In the frame of the giant-spin Hamiltonian description of the system, it has been possible to evidence the presence of sixth-order terms of the magnetic anisotropy. It has also been possible to ascribe the striking angular dependence of the resonance field observed at 115 GHz in the hard plane to an accidental balancing of the fourth- and sixth-order transverse anisotropy contributions. These terms play a key role in the quantum tunneling of the magnetization which dominates the dynamics of SMMs at low temperature. To understand their physical origin a simplified multispin Hamiltonian has been employed based on ligand field calculations and the observed crystal structure. For the first time it has been evidenced that the fourth-order transverse anisotropy is directly connected to the tilting of the single-ion easy axes. Interestingly higher-order terms have a more complex behavior, and subtle changes in the tilting angle produce significant variations in the ratio between sixth- and fourth-order anisotropy and in the resulting tunnel splitting.

This study shows that the effective giant-spin Hamiltonian of complex systems can be rationalized using a simple multispin Hamiltonian to establish magnetostructural correlations that open the perspective to tailor on design the magnetic anisotropy of SMMs up to higher orders.

Experimental Section

Synthesis. Crystals of $[Mn_{12}O_{12}(^tBu-CH_2CO_2)_{16}(CH_3OH)_4]\cdot CH_3OH$ were obtained in two steps following the procedure reported in the literature.[34] Mn12Ac was used in the standard ligand substitution reaction in toluene by exploiting the formation of an azeotrope with acetic acid. Recrystallization from CH_2Cl_2 and MeCN produced small crystals of $[Mn_{12}O_{12}(^tBu\text{-}CH_2CO_2)_{16}(H_2O)_4]\cdot CH_2Cl_2\cdot MeCN$[50] that were redissolved in MeOH and Et_2O with a small addition of *tert*-butylacetic acid. A precipitate formed after a few days. The procedure was then repeated a second time to afford larger (ca. 0.5 mm^3) rod-shaped crystals.

X-ray Analysis. A freshly synthesized single crystal of dimension ($0.1 \times 0.1 \times 0.6$ mm^3) was mounted on a goniometric head and investigated at 150 K with an Xcalibur3 (Oxford Diffraction) diffractometer using Mo Kα radiation ($\lambda = 0.71073$ Å). Data reduction was accomplished using CRYSALIS.RED.[51] The structure was solved by direct methods (SIR97)[52] which gave the positions of all the non-hydrogen atoms. The structure was refined against F_0^2 using SHELXL-97 program[53] implemented in the WINGX suite.[54] Anisotropic thermal factors were used for all the non-hydrogen atoms of the cluster moiety, whereas those of methanol solvent molecule were kept isotropic. Hydrogen atoms were added in calculated positions and allowed to ride on their parent atoms. Details of crystal data collection and structure refinement are collected in Table 1.

Table 1. Crystal Data and Structure Refinement for Mn12^{t}BuAc

empirical formula	$C_{101}H_{196}Mn_{12}O_{49}$
formula weight	2853.9
temperature	150(2) K
wavelength	0.71073 Å
crystal system	tetragonal
space group	$I\bar{4}$
unit cell dimensions	$a = 21.481(5)$ Å, $\alpha = 90°$ $b = 21.481(5)$ Å, $\beta = 90°$ $c = 15.148(5)$ Å, $\gamma = 90°$
volume	6990(3) Å^3
Z	2
density (calculated)	1.356 Mg/m^3
absorption coeff.	1.119 mm^{-1}
$F(000)$	2972
crystal size	$0.1 \times 0.1 \times 0.6$ mm^3
θ range	4.24 to 26.08°
index ranges	$-25 \le h \le 15$, $-20 \le k \le 25$, $-10 \le l \le 18$
reflns collected	10255
independent reflns	5344 [R(int) = 0.0296]
completeness $\theta = 25.00°$	92.5%
refinement method	full-matrix least-squares on F^2
data/restraints/param	5344/1/379
GOF on F^2	1.167
Final R [$I > 2\sigma(I)$]	$R1 = 0.0568$, $wR2 = 0.1450$
R indices (all data)	$R1 = 0.0686$, $wR2 = 0.1632$
absolute structure param	−0.04(3)
largest difference peak and hole	1.333 and −0.557 eÅ^{-3}

HF-EPR Spectra. A home made single-pass multifrequency spectrometer was used.[55,56] The main magnetic field, which is vertical, is obtained from a superconducting magnet (Cryogenic Consultant) with a maximum field of 12 T at 4.2 K. This maximum field value determined the highest frequency to be used to observe the perpendicular transitions. The frequency source used was a Gunn oscillator operating at 115 GHz (Radiometer Physics). The detection of the light transmitted through the sample is performed with a hot electron InSb bolometer (QMC Instruments), working at liquid helium temperature. For single-crystal measurements a dedicated sample holder is used, allowing a complete rotation (360°) of the sample around the horizontal axis. A very important property of this holder is to enable operating in Faraday configuration. HF-EPR spectra were recorded on several single crystals (one at a time) with the largest dimension (along the fourth-fold axis) of the order of 1 mm, while the two other ones were slightly smaller (~0.5 mm).

Acknowledgment. We acknowledge financial support from the EC through the Human Potential Program RTN-QUEMOL-NA (FP6-504880), NE-MAGMANET (FP6−NMP3-CT-2005-515767), and Transnational Access Specific Support Action (RITA-CT-2003-505474), Italian MURST grants, and German DFG (SPP1137). We also greatly acknowledge Dr. Hogni Weihe (University of Copenhagen) for his EPR simulation softwares as well as his kind help in using it.

Supporting Information Available: Crystallographic details in CIF format, scheme of the crystal packing of Mn12^{t}BuAc

(50) Soler, M.; Wernsdorfer, W.; Sun, Z. M.; Huffman, J. C.; Hendrickson, D. N.; Christou, G. *Chem. Commun.* **2003**, 2672−2673.
(51) *Crysalis RED*, versions 1.171.29.9; Oxford Diffraction Ltd: Oxford, U.K.
(52) Altomare, A.; Burla, M. C.; Camalli, M.; Cascarano, G.; Giacovazzo, C.; Guagliardi, A.; Moliterni, A. G. G.; Polidori, G.; Spagna, R. *J. Appl. Cryst.* **1999**, *32*, 115−119.
(53) Sheldrick, G. M. *SHELX-97, an Integrated System for Solving and Refining Crystal Structure From Diffraction Data;* University of Göttingen: Göttingen, Germany, 1997.
(54) Farrugia, L. J. *J. Appl. Crystallogr.* **1999**, *32*, 837.
(55) Muller, F.; Hopkins, M. A.; Coron, N.; Grynberg, M.; Brunel, L. C.; Martinez, G. *Rev. Sci. Instrum.* **1989**, *60*, 3681.
(56) Barra, A.-L.; Brunel, L. C.; Robert, J. B. *Chem. Phys. Lett.* **1990**, *165*, 107.

(Figure S1), selected bond lengths and angles (Table S1), temperature dependence of the axial EPR spectra (Figure S2), additional results of multispin Hamiltonian calculations (Figures S3, S4, S5, and Table S2), and analytical treatment in the high field limit. This material is available free of charge via the Internet at http://pubs.acs.org.

JA0717921